

**The Effects of a Navier-Slip Boundary Condition on the Flow of  
Two Immiscible Fluids in a Microchannel**

by

Charles Edward Fisher III

A Project Report

Submitted to the Faculty

of the

WORCESTER POLYTECHNIC INSTITUTE

In partial fulfillment of the requirements for the

Degree of Master of Science

in Applied Mathematics

by

---

April 2013

Approved:

---

Professor Burt S. Tilley, Capstone Advisor

---

Professor Bogdan Vernescu, Department Head

## Abstract

We consider the flow of two immiscible fluids in a thin inclined channel subject to gravity and a change in pressure. In particular, we focus on the effects of Navier slip along the channel walls on the long-wave linear stability. Of interest are two different physical scenarios. The first corresponds to two incompressible fluid layers separated by a sharp interface, while the second focuses on a more dense fluid below a compressible gas. From a lubrication analysis, we find in the first scenario that the system is stable in the zero-Reynolds number limit with the slip effects modifying the decay rate of the stable perturbation. In the case of the Rayleigh-Taylor problem, slip along the less dense fluid wall has a destabilizing effect. In the second scenario, fluid inertia is pertinent, and we find neutral stability criteria are not significantly affected with the presence of slip.

## Acknowledgements

I would first like to thank Professor Burt Tilley for guiding me through one of the most difficult years I have known. His advice, both academic and non-academic has been the driving force I needed to achieve several triumphs in a year full of obstacles. Professor Tilley has done an excellent job of teaching me how to work towards an answer myself and utilize countless resources.

The faculty and friends I have made during my studies at WPI will always be held in high gratitude. I would like to thank Professor Mayer Humi and Professor Homer Walker who both furthered my knowledge of MATLAB and Numerical Analysis. I would also like to thank Professor Konstatin Lurie for taking the time to do an independent study. The lectures and work with William Sanguinet were an excellent beginning to my time at WPI.

I would also like to thank my undergraduate advisor, Peter Staab for instilling in me a love of Applied Mathematics and taking me along to several local and national conferences. I would not have experienced the vast amount of mathematical research if it was not for you and Mark Maggio. From Times Square to Magic Squares, I enjoyed it all.

Finally, I would thank my wife Erica Fisher and my four sons, Tyler, Seth, Ewan and Lucas. You have been my rock, my inspiration and my love through all of this. I never expected to find myself at the age of 35 but you helped me achieve it. I dedicate this work to you.

# Contents

<b>1</b>	<b>Introduction</b>	<b>1</b>
1.1	Laminar and Creeping Flow on a Surface . . . . .	1
1.2	Flow Over Microchannels . . . . .	4
1.3	Rarefaction Effects on Flow . . . . .	5
<b>2</b>	<b>Formulation of the Equations</b>	<b>9</b>
2.1	Given Equations . . . . .	9
2.2	Non-dimensionalization . . . . .	11
<b>3</b>	<b>Perturbation Analysis</b>	<b>13</b>
3.1	Liquid-Liquid . . . . .	15
3.2	Liquid-Gas . . . . .	18
<b>4</b>	<b>Long Wave Linear Stability Analysis</b>	<b>24</b>
4.1	Analysis of the Liquid-Liquid Case . . . . .	24
4.2	Analysis of Liquid-Gas Case . . . . .	26
<b>5</b>	<b>Conclusion and Planned Future Work</b>	<b>31</b>

# 1 Introduction

Thin or laminar fluid flow is applicable to many situations. If scaled correctly the same thin fluid model can accurately describe corneal fluid on an eyeball or glacier and ice sheet flows. Recent advent of nano technology and the requirement of minimizing devices has forced a growing interest in microscale fluid dynamics.

The problem investigated in this work stems from Segin et al [27], [26] and looks at dual laminar flow of a compressible and incompressible fluid in a microchannel (see figure 1). We investigate the region where the flow is fully developed so entrance and exit phenomena do not need to be incorporated. We include the addition of the Navier Slip boundary condition  $\beta_2$  on the second phase (gaseous) wall. This boundary condition will be directly related to the accommodation coefficient, a numerical value between 0 and 1 that is in reference to the type of slip which depends on the physical properties of the wall. An ideal wall which is perfectly smooth at the molecular level produces specular reflection which implies the angle of incidence and reflection of the molecules colliding with the wall are identical and therefore the molecules conserve their tangential momentum. The accommodation coefficient for specular reflection is small, close to zero. Diffusive or complete reflection occurs on a rough wall which impedes the angle of incidence and creates friction has an accommodation coefficient closer to one. We will derive the slip coefficient for both walls but ultimately set  $\beta_1 = 0$ . The advantage of including both in the derivation is for future possible analysis of dual compressible gas flow.

In order to introduce the Navier Slip boundary condition, we shall follow the formulation of  $\beta$  prescribed in [3]. Barber considers flow past a sphere but the formulation for slip is physically comparable to our case.

## 1.1 Laminar and Creeping Flow on a Surface

We first look at works done on laminar and creeping flow on a surface. While most of some of this work is performed on a smooth inclined plane, we are also interested when protrusions or rough surfaces create additional effects. Included are expositions on gravity induced flow as well as surface force driven flow.

Thin fluid flow analysis is typically performed using asymptotics and linear stability as done by D.J. Benney [5]. Benney looked at a single film

flowing down an inclined plane. Using the Navier-Stokes equations along with the typical no penetration and no slip boundary conditions, Benney forms his model in terms of stream functions and derives equations for interface and pressure. He then considers a small perturbation on  $\psi$  and  $P$  and uses the boundary conditions again to show breaking wave signatures. The motion is viscous, much like magma flow or glacial ice flow. He also notes conditions under which a given disturbance will deform and the result is unstable. By utilizing linear stability theory and assuming a steady state solution he arrives at a parabolic equation for the interface. Investigating small perturbations about the neutral conditions leads to an eigenvalue problem which results in unstable waves and similarities to Burger's equation. Benney's paper does not take slip into consideration but many analysis of this type have subsequently followed.

Buckingham and Bertozzi [6] looked at travelling waves on an inclined plane, the Benney problem only uphill by a surface stress, or Marangoni force with a Navier-Slip boundary condition imposed. Similar to Benney, nondimensionalization and perturbation expansion is performed and solved with the appropriate boundary conditions. The three cases investigated are when gravity dominates, which is the Benney problem above, when the Marangoni force dominates and when the two are in balance. Each case is scaled dependent on the respective case and the classical linear stability method is used. The writers are interested in contact lines at  $h = 0$ . They note that when the flow is upstream the wave approaches a constant height whereas the downstream flow leads to a traveling wave. The slip coefficient in this case is restricted to a small neighborhood of the contact line. They then use a Frobenius expansion and show that the asymptotic series defines a two parameter family of formal solutions. Numerically they reduce the problem to a planar vector field and use Poincare sections for the analysis. The numerical data supports the analytical solutions well but the analysis does not consider slip over the entire surface of the flow.

Cassie and Baxter [7] analysed laminar flow on a porous surface akin to textile surfaces defined by uneven fibers. Using conservation of energy, they describe the change in interfacial energy between liquid and air. The net energy equation is written in terms of the contact angle and a descriptive analysis of advancing and receding contact angles is achieved. This allows for a deduction of a roughness factor that influences the contact angle based on geometry. Using this analysis, they successfully predict advancing and receding contact angles on fiber geometry. An experiment is designed to

validate the analysis and a discussion of textile geometrical design is given. One highlight is that the severity of the contact angle can cause a water drop to roll off the surface instead of soaking into it. This subject is then extended to animal coat and feather designs and a detailed explanation of how this explains the wetting or lack of wetting with regards to a duck. The paper suggests that designing rain resistant clothing should focus more on geometry and less on coatings to prohibit wetting.

Further investigation has been done into geometry based development of slip flow. Davis and Lauga [10] showed the effect of friction on pressure requirements. The work introduces a Navier-slip boundary condition and shows how slip can reduce friction in microchannel flow. Looking at superhydrophobic surfaces they offer an explanation of how fluid contact on solid angles occurs. The gas pockets that develop can distort flow streamlines depending on the geometry, i.e. too much protrusion causes more friction than a planar surface. They find the critical angle of the protruding bubble at which the benefits are hindered which turns out is 65 degrees. By defining a stream function and using shear flow before the bubble they define the equation for a single bubble and then assumed periodicity to introduce a series of bubbles. This analysis leads to a range of optimal effective slip between -30 (convex bubble) and 40 (concave bubble) degrees. This defines the existence of a flow asymmetry between convex and concave bubble.

Lauga and Stone [18] looked at slip flow in a cylindrical channel. Two elementary configurations were considered using alternating areas of no slip and perfect slip. One setup consisted of lateral breaks in the slip condition and the other longitudinal sections of slip and no slip down the walls. The longitudinal analysis was done analytically and the lateral was done numerically. They found that when the slip percentage was small the effective slip length decreased more in the longitudinal than the lateral. Also when the percentage was large the longitudinal diverged slower than the lateral. A scaling is then introduced such that both models approach each other in performance and compared to experimental data. However, quickly noted was the requirement that the experimental data is only valid if the correction due to slip flow is much greater than the experimental error. So the validation could only be done in microchannels of radius approximately 1 mm. They were able to model slip effect taken from experimental data but cautioned against the inability of the model to consider the surface dimension effects caused by the micro-bubbles which were causing the slip in the experimental data.

Fuellebois and co-workers [15] considered an area of slip on a surface of a thin channel and obtained bounds on the effective slip length. This work is similar to that of Stone and Lauga [18] but only considers longitudinal flow. Doing this they found that modifying surface profile can induce novel wetting properties and achieve the goals set above. They also noted the Cassie state, when the texture is filled with gas can drastically amplify hydrophobicity. Determination was once again made that the effective slip length is directly related to the fraction of solid in contact with the liquid, thus the gas.

## 1.2 Flow Over Microchannels

In a further look at geometry induced slip flow, Sbragaglia and Prosperetti also investigated the random allocation of nano bubbles that arise on boundary walls and their induced effect on slip length [24]. These bubbles satisfied a partial slip condition and statistical analysis did indeed show that they exist and are created at random. The statistical analysis gives a random allocation to nanobubbles. The problem connects the laminar flow problem of Cassie [7] and Davis [10] with flow in a microchannel as in Sbragaglia [25].

In continuing analysis on the effect of geometry implications on slip flow, Ybert and co-workers [32] looked at defining effective slip length based on structure and texture properties. Their problem was interested in flow over a surface with periodic disturbances such as small perpendicular or parallel channels or pillars. This analysis of stripes, pillars and holes provides for a detailed table listing functions for effective slip lengths. It then goes onto suggest height boundaries of certain structures in order to optimize results.

Ng and Wang [22] [21] looked at the effect of periodic slats at the wall boundaries and bidimensional surfaces on Stokes shear flow. Similar to [32] they considered both transverse flow and longitudinal flow. One major result is that the superhydrophobic state is effective only when pressure is below a certain threshold so the no-shear interface is not positioned too deeply in the voids.

The recent development of MEMS and the microchannels with which they utilize pertains to several works on this microchannel flow. Currently a significant pressure difference must exist in order for the transport through nano size devices [25]. Since superhydrophobic surfaces offer slip on the boundary, less pressure is needed to induce flow. Sbragaglia and Prosperetti confirm this using perturbation theory [25] and calculate a correction to the effective slip length based on capillary effects. The geometry of their problem

is similar to [32], [22], [21] but here they only look at what Ng et al defined as longitudinal flow (i.e. in the direction of the microchannels)

Teo and Khoo [28] consider a similar problem on transverse flow over a series of channels. Here they once again validate that the geometrical design of the grooves in the surface directly effect the slip length. Furthermore they show that laminar flows report a decrease in flow resistance.

In a further exposition of the effect these nanobubbles would have on flow, Chakraborty et al [9] looked at the slip flow at the entrance region of the microchannel. Similar to the work done by Sbragaglia, [24], [25] Chakraborty's analysis is on longitudinal flow in a microchannel however here they look at developing flow and the effect that the allocation of nanobubbles has on developing and fully developed flow. Chakraborty et al derive an analytical method used to assess accuracy, convergence and effectiveness of numerical simulations and solutions of pressure driven flow. They find that depending on the nanobubble thickness, developing flow and fully developed flow show a negligible difference in the friction factor characteristics. This has implications on the design and construction of said systems if maintaining a constant friction factor is required.

### 1.3 Rarefaction Effects on Flow

Yuhong, Barber and Emerson [33] independently confirm the phenomena of inverted velocity profiles that arise in cylindrical Couette flow cases as first reported by Einzel et al [14]. They find that the phenomena is dependent on the movement of both cylinders and show that the fluid indeed develops an inverted velocity profile under certain conditions. Note the word inverted here implies an increasing velocity as the flow moves from the rotating inner cylinder towards a stationary outer cylinder. Unlike the work of Tibbs et al, this paper used Maxwell's slip-flow model to verify the phenomena with a different approach. The findings are consistent with Tibbs et al[29] and the Direct Simulation Monte Carlo methods performed previously in that paper.

Arkilic and co-workers [2] consider two dimensional flow in a microchannel. They introduce the Navier-Slip condition and assume a time invariant, constant viscosity, isothermal system and ignore body forces. The isothermal assumption is shown to be good for low Mach number flows in long uninsulated microchannels. Utilizing perturbation expansion they explain the different flow regimes in terms of orders of epsilon. For instance, the microflow regimes characterized by (Mach Number, Reynolds Number)  $O(\epsilon, \epsilon)$ ,

$O(1,1)$  and  $O(\epsilon,1)$  are all appropriately modeled by perturbation analysis. Using continuity and the appropriate boundary conditions they arrive at equations for velocity and a zeroth-order pressure equation. The results indicate a parabolic streamwise velocity profile and they offer examples of different profiles dependent on geometry and physical attributes. The analysis is compared with and lines up well with preexisting experimental data.

This brings the investigation to the analysis of flow in microchannels in a closed duct. Using analytical approaches and working from the need for microchannels in MEMS device manipulation, Duan and Muzychka looked at slip flow in microchannels of several geometric designs including rectangular and elliptical ducts [11], [12]. Their method used scaling to compare friction with pressure to arrive at flows dominated by viscous effects thus density changes may be significant. Using the respective channel geometry, for instance, elliptic cylinder coordinates and separation of variables, they were able to arrive at a solution to the problem after introducing a Navier-Slip boundary condition. Both papers develop a mass flow equation and subsequently let  $Kn$  go to zero to compare slip flow with continuum flow. The model was then developed for predicting the Poiseuille number and may be used to predict mass flow rate and pressure distribution. They also showed that slip flow decreases as rarefaction effects become greater, i.e. the ratio of slip flow over continuum flow goes from 1 to 0.5 as  $Kn$  goes from 0 to 0.1. Also the geometry of the channel once again influenced the flow as a circle had a 0.6 flow ratio and an ellipse was closer to 0.45. They show that rarefaction increases mass flow and the effect becomes more significant when the pressure ratio decreases.

In a similar paper they then extended their work to analyze the developing flow at the entrance of both types of channels [13]. After a comprehensive explanation of the Poiseuille number and the definition of the region to be analyzed, namely the length of the channel required to achieve fully developed flow, the equations are written out in polar coordinates. Using continuity and momentum they arrive at an equation for the velocity distribution. They introduce Navier-Slip at the walls and arrive at an eigenvalue problem similar to Bessels equation. They then analyse the velocity distribution for various distances away from the entrance region. Ultimately this allows for the suggestion that using the hydrodynamic entrance length for design of a microfluidic device is perhaps optimal. The momentum equation is then integrated to arrive at the pressure equation and then to the friction function. The same analysis is then done with parallel plates and cartesian

coordinates and a similar velocity distribution is achieved. This allows for validation of both models with several experimental results.

Renksizbulut et al[23] looked at a numerical investigation of rarefied gas flow and heat transfer in a rectangular duct in three dimensions. Their investigation was limited to the bounds of  $0.1 < Re \leq 10$  and  $Kn \leq 0.1$ . They found a monotonic reduction in the friction factor and Nusselt number due to rarefaction effects. They also noted that in the fully developed region both wall friction and heat transfer were significantly affected by rarefaction and the aspect ratio of the channel.

Similarly Hettiarachchi and coworkers [17] also worked on 3 dimensional laminar slip mass driven flow in a rectangular duct with constant wall temperature. They introduce a slip and temperature jump at the wall and deal with both the tangential and energy accommodation coefficients. The slip due to the temperature gradient adjacent to the wall is second order and thus negligible. They use a preconditioned GMRES method for numerical solution of the flow. They noted that the rarefaction effect decreased velocity and pressure gradients in the channel resulting in a considerable reduction in the friction factor as well as the amount of slip decreases as flow approaches a fully developed region. The paper then goes on to discuss temperature related effects and distribution in developing and fully developed flow. Zade et al [34] investigated the same geometry but looked at the effect of the developing flow and fully developed flow on the Knudsen and Nusselt numbers respectively.

Muzychka and Yoranovich [20] analysed asymptotic results for short and long duct microchannels. They developed a simple model for predicting the friction factor the requires only the aspect ratio and the dimensionless duct length. Their method predicts developing flow within 10%.

Morini and others [19] developed a criterion for experimental validation of models dealing with these various channel-duct systems. Their work began with the analysis of the friction factor for incompressible rarefied gas flow. They show that it was possible to calculate a minimum value of  $Kn$  for which the rarefaction effects could be observed. Additionally they investigate past literature using the bounds that are derived. Furthermore, they determined the pressure drop through microchannels to obtain experimental data able to validate the classical slip flow models. Thus they noted that only microchannels having a depth of 1-20  $\mu m$  can be employed.

Gu and Emerson [16] expanded the moment method to accurately describe any non-equilibrium phenomena in planar Couette flow as well as

Poiseuille flow. As the  $Kn$  number increases, more moments must be included in order to accurately describe any non-equilibrium phenomena occurring from rarefaction effects. Thus they investigate Cercignani's work in 1988 [8] and the H-theorem as well as the validity of Grad's 13 moment equations developed in 1949 to deal with this problem. Gu and Emerson formulate an additional 13 equations for a culmination of 26 moment equations to accurately describe any non-equilibrium phenomena. This allows better numerical modelling into the upper transition regime.

The work done by Chu [1] also utilizes linearized stability theory. Starting with the Orr-Sommerfeld equation and the basic velocity profile of the flow, a Navier-Slip boundary condition is introduced. Then a Chebyshev polynomial expansion is performed to accommodate a Spectral Method to solve the eigenvalue problem. Numerical results are validated with data from prior work and a comparison of critical Reynolds numbers and wavelengths are reviewed. The data shows that the slip velocity degrades the flow stability significantly. A comparison of short and long wave instabilities is examined and the slip condition is determined to be by the increasing Navier slip. Detailed reasoning for this phenomena is stated as unknown.

In an examination of quasi-two-dimensional magnetohydrodynamic flow modeled as Hartmann flow with Navier-Slip boundary condition, Vetcha et al [31] use the Orr-Sommerfeld equation and a Chebyshev/Spectral method similar to above. The flow is assumed to be fully developed and the numerical work is done in MATLAB. Using modal stability analysis, the flow is defined to be linearly unstable if there exists at least one eigenvalue with a positive imaginary part. Both symmetric, slip on both sides and asymmetric, slip only on one side are examined. In symmetric slip, small slip lengths are strongly stabilizing. However the same result is not evident in asymmetric flow. Also noted is that in the absence of a magnetic field, slip below a certain value destabilizes flow. However, this analysis is limited to a single fluid and suggests a look into the effects on a two fluid system.

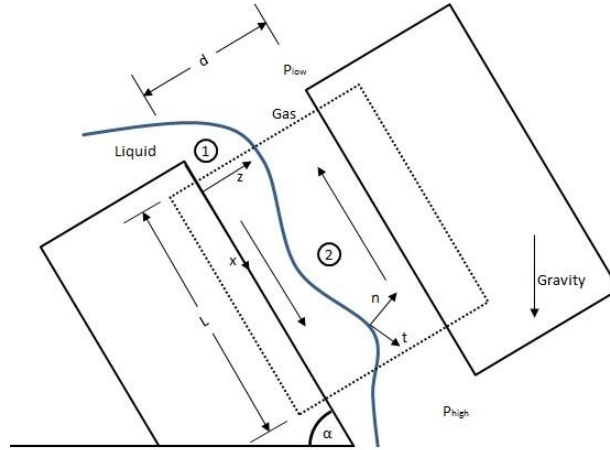


Figure 1: Description of the problem of interest. The plate on the left is coated by a liquid driven down by gravity. The dashed box is the considered domain as we assume fully developed flow for both fluids. The gas is driven up counter-currently to the fluid due to a pressure drop. Shown is the fluid normal and interfacial tangent along  $z = h(x, t)$

## 2 Formulation of the Equations

### 2.1 Given Equations

We consider a microchannel such that the height,  $d$  is much less than the length  $L$ . We assume isothermal conditions in order to simplify implications of the ideal gas law. Furthermore  $\mathbf{n}$  is the unit normal pointing from the incompressible liquid hereby referred to as phase 1 into the compressible gas, phase 2 and  $\mathbf{t}$  will be the unit vector at the interface of phase 1 and phase 2. We begin our analysis with the continuity and the Navier-Stokes equations as well as an equation of state for the gas that depends on flow as well as density. We later assume that we are dealing with both fluids defined as liquids to compare the two cases. To do so we simply take  $\rho$  as a constant

and no longer need the equation of state for the phase 2 fluid.

$$\begin{aligned}\nabla \cdot \mathbf{u}^{*(1)} &= 0 \\ \rho_1^* \left( \frac{\partial \mathbf{u}^{*(1)}}{\partial t^*} + \mathbf{u}^{*(1)} \cdot \nabla \mathbf{u}^{*(1)} \right) &= -\nabla p^{*(1)} + \rho_1^* \mathbf{g} + \mu_1^* \nabla^2 \mathbf{u}^{*(1)} \\ \rho_2^* + \nabla \cdot \rho_2^* \mathbf{u}^{*(2)} &= 0 \\ \rho_2^* \left( \frac{\partial \mathbf{u}^{*(2)}}{\partial t^*} + \mathbf{u}^{*(2)} \cdot \nabla \mathbf{u}^{*(2)} \right) &= -\nabla p^{*(2)} + \rho_2^* \mathbf{g} + \mu_2^* \left( \nabla^2 \mathbf{u}^{*(2)} + \frac{1}{3} \nabla (\nabla \cdot \mathbf{u}^{*(2)}) \right) \\ p^*(2) &= K^* \rho_2^*\end{aligned}$$

Above we define  $\mathbf{u}^*$  as the velocity vector, and in each phase  $i$ ,  $\rho_i^*$  the density,  $\mu_i^*$  the viscosity,  $p^{*(i)}$  the pressure and  $g$  the force due to gravity. The superscripts correspond to the fluid domain, the stars imply dimensional variables and the final equation follows from the ideal gas law assumes isothermal conditions, i.e. ( $\rho V = nRT$ ).  $K^*$  represents the square of the local speed of sound in the gas layer and is defined as  $K^* = RT^*/M$  such that  $R$  is the universal gas constant,  $T^*$  the dimensioned ambient temperature and  $M$  is the molecular weight of the gas. The derivation of the formal equations will be carried out with an arbitrary angle of inclination represented by  $\alpha$ .

Although the velocities  $\mathbf{u}^{*(i)} = (u^{*(1)}, w^{*(1)})$  satisfy the no-penetration boundary condition we will now introduce the Navier-Slip boundary condition on the channel walls. Navier's Slip law

$$\dot{u}t = \beta \hat{t} \ddot{T} n$$

In order to accurately incorporate the slip boundary condition into the problem we define the slip coefficient  $\beta$  as follows:

$$\beta = \frac{\mu}{\left(\frac{2-\sigma}{\sigma}\right) \lambda}$$

$\mu$  once again is viscosity,  $\lambda$  is the mean free path and  $\sigma$  is our accommodation coefficient. The balance of normal stress, balance of tangential stress, continuity of normal and tangential components of velocity and kinematic condition at  $z^* = h^*(x^*, t^*)$  are still satisfied. This gives the following equa-

tions:

$$[\mathbf{n} \cdot \mathbf{T}^* \cdot \mathbf{n}] = \gamma^* \kappa^* \quad (1)$$

$$[\mathbf{t} \cdot \mathbf{T}^* \cdot \mathbf{n}] = 0 \quad (2)$$

$$[\mathbf{u}^* \cdot \mathbf{n}] = 0 \quad (3)$$

$$[\mathbf{u}^* \cdot \mathbf{t}] = 0 \quad (4)$$

$$h_{t^*}^* + u^* h_{x^*}^* - w^* = 0 \quad (5)$$

$\mathbf{T}^*$  is the stress tensor,  $\gamma^*$  is the interfacial tension between the liquid and gas and  $\kappa^*$  is twice the mean curvature of the interface defined such that  $\kappa^* = -h_{x^* x^*}^* (1 + h_{x^*}^{*2})^{-3/2}$ .

## 2.2 Non-dimensionalization

We now scale our lengths on the channel height  $d$ , densities on the fluid density  $\rho_1$ , time on  $t^* dg / \nu_1^*$ , pressure on  $p^{*(i)} / \rho_1^* dg$  and velocities by  $d^2 g / \nu_1^*$  where  $\nu_1^* = \mu_1^* / \rho_1^*$  is the kinematic viscosity of phase 1. We can separate the analysis into the two cases we mentioned above, the liquid-liquid problem and the liquid-gas problem. So, we then get the following system for the liquid-liquid problem:

$$\nabla \cdot \mathbf{u}^{(i)} = 0 \quad (6)$$

$$\mathbf{Re}_1 \left\{ \frac{\partial \mathbf{u}^{(i)}}{\partial t} + \mathbf{u}^{(i)} \cdot \nabla \mathbf{u}^{(i)} \right\} = -\nabla p^{(i)} + \hat{\mathbf{g}} + \nabla^2 \mathbf{u}^{(i)} \quad (7)$$

When the phase 2 fluid is compressible the equations are given by

$$\nabla \cdot \mathbf{u}^{(1)} = 0 \quad (8)$$

$$\mathbf{Re}_1 \left\{ \frac{\partial \mathbf{u}^{(1)}}{\partial t} + \mathbf{u}^{(1)} \cdot \nabla \mathbf{u}^{(1)} \right\} = -\nabla p^{(1)} + \hat{\mathbf{g}} + \nabla^2 \mathbf{u}^{(1)} \quad (9)$$

$$\rho_t + \nabla \cdot \rho \mathbf{u}^{(2)} = 0 \quad (10)$$

$$\mathbf{Re}_1 \rho \left\{ \frac{\partial \mathbf{u}^{(2)}}{\partial t} + \mathbf{u}^{(2)} \cdot \nabla \mathbf{u}^{(2)} \right\} = -\nabla p^{(2)} + \rho \hat{\mathbf{g}} + \mu \left\{ \nabla^2 \mathbf{u}^{(2)} + \frac{1}{3} \nabla (\nabla \cdot \mathbf{u}^{(2)}) \right\} \quad (11)$$

$$p^{(2)} = K \rho \quad (12)$$

$\rho$  and  $\mu$  are the density and viscosity ratios of the second phase over the first respectively.  $K = K^*/dg$ ,  $\text{Re}_1 = gd^3/\nu_1^{*2}$  is the Reynolds number of phase 1,  $\hat{\mathbf{g}}$  is the unit vector in the direction of gravity and the velocities are the simply  $\mathbf{u}^{(i)} = (u^{(i)}, w^{(i)})$ . Also  $\gamma = \gamma^*/\rho_1^* d^2 g$ . The boundary conditions on the channel walls and conditions (2.1.1)-(2.1.5) are

$$\mathbf{u}^{(1)} = \beta_1 \mathbf{u}_z \text{ on } z = 0 \quad (13)$$

$$\mathbf{u}^{(2)} = -\beta_2 \mathbf{u}_z \text{ on } z = 1 \quad (14)$$

$$[\mathbf{n} \cdot \mathbf{T} \cdot \mathbf{n}] = \zeta \kappa \quad (15)$$

$$[\mathbf{t} \cdot \mathbf{T} \cdot \mathbf{n}] = 0 \quad (16)$$

$$[\mathbf{u} \cdot \mathbf{n}] = 0 \quad (17)$$

$$[\mathbf{u} \cdot \mathbf{t}] = 0 \quad (18)$$

$$h_t + u h_x - w = 0 \quad (19)$$

When we consider the profile of  $\mathbf{u}^{(2)}$  it is worth noting that the local derivative with respect to  $\xi$  close to the wall will be negative. Instead of allowing the negative sign to be absorbed into  $\beta_2$  we will utilize the sign to further understand the behavior and effects it induces on our system below. For the general case analysis we will consider a system on the order of the classical air/water relationship.

Furthermore, we have that the constant flow rate for the channel is noted  $Q$  and is as such:

$$\int_0^1 u \, dz = Q$$

### 3 Perturbation Analysis

From Batchelor [4] we know that for air-water, the density and viscosity ratios are  $\rho_2/\rho_1 = 12 \times 10^{-4}$  and  $\mu_2/\mu_1 = 2 \times 10^{-2}$ . Also, we define the aspect ratio of the channel width to length as  $\epsilon$ . Thus  $\rho_2/\rho_1$  is of the order  $\epsilon^2$  and  $\mu_2/\mu_1$  is on the order of  $\epsilon$ . Similarly, if we look at the ratio of the two Reynolds numbers we get

$$\frac{\text{Re}_1}{\text{Re}_2} = \frac{dU_1/\nu_1^*}{dU_2/\nu_2^*} = \frac{\nu_2^* U_1}{\nu_1^* U_2} = \frac{1}{\epsilon} \frac{U_1}{U_2}$$

Note that  $U_1$  and  $U_2$  are the characteristic velocities of the liquid and gas respectively. This implies that the order of the tangential velocity scale is of  $O(1)$ . We will now scale the spatial variables and introduce a slow time scale,  $\xi = \epsilon x$ ,  $\zeta = z$  and  $\tau = \epsilon t$ . This gives us the final formulation for our system of equations such that we can begin our analysis.

$$\epsilon u_\xi^{(1)} + w_\zeta^{(1)} = 0 \tag{20}$$

$$\begin{aligned} \text{Re}_1 \epsilon \left[ u_t^{(1)} + u^{(1)} u_\xi^{(1)} + \frac{1}{\epsilon} w^{(1)} u_\zeta^{(1)} \right] = \\ -\epsilon p_\xi^{(1)} + \cos \alpha + \epsilon^2 \left( u_{\xi\xi}^{(1)} + \frac{1}{\epsilon^2} u_{\zeta\zeta}^{(1)} \right) \end{aligned} \tag{21}$$

$$\begin{aligned} \text{Re}_1 \epsilon \left[ w_t^{(1)} + u^{(1)} w_\xi^{(1)} + \frac{1}{\epsilon} w^{(1)} w_\zeta^{(1)} \right] = \\ -\epsilon p_\zeta^{(1)} + \sin \alpha + \epsilon^2 \left( w_{\xi\xi}^{(1)} + \frac{1}{\epsilon^2} w_{\zeta\zeta}^{(1)} \right) \end{aligned} \tag{22}$$

$$\epsilon \rho_\tau + \epsilon(\rho u^{(2)})_\xi + (\rho w^{(2)})_\zeta = 0 \quad (23)$$

$$\begin{aligned} \text{Re}_1 \epsilon^2 \rho \left[ \epsilon u_t^{(2)} + \epsilon u^{(2)} u_\xi^{(2)} + w^{(2)} u_\zeta^{(2)} \right] &= -\epsilon p_\xi^{(2)} + \\ &\epsilon^2 \rho \cos \alpha + \frac{\mu}{3} \left( 4\epsilon^3 u_{\xi\xi}^{(2)} + 3\epsilon u_{\zeta\zeta}^{(2)} + \epsilon^2 w_{\zeta\zeta}^{(2)} \right) \end{aligned} \quad (24)$$

$$\begin{aligned} \text{Re}_1 \epsilon^2 \rho \left[ \epsilon w_t^{(2)} + \epsilon u^{(2)} w_\xi^{(2)} + w^{(2)} w_\zeta^{(2)} \right] &= -\epsilon p_\zeta^{(2)} + \\ &\epsilon^2 \rho \sin \alpha + \frac{\mu}{3} \left( 4\epsilon^3 w_{\xi\xi}^{(2)} + 3\epsilon^3 w_{\zeta\zeta}^{(2)} + \epsilon^2 u_{\zeta\zeta}^{(2)} \right) \end{aligned} \quad (25)$$

We can note here that the liquid-liquid problem can be analyzed from here by letting  $\rho$  be a constant. We will begin the analysis with this case and then extend it to the more general case in the following section. Following the classical method of laminar fluid flow analysis, we will now introduce the following perturbation expansions

$$\begin{aligned} u^{(1)}(\xi, \zeta, \tau) &= u_0^{(1)}(\xi, \zeta, \tau) + \epsilon u_1^{(1)}(\xi, \zeta, \tau) + \dots \\ w^{(1)}(\xi, \zeta, \tau) &= \epsilon \{ w_0^{(1)}(\xi, \zeta, \tau) + \epsilon w_1^{(1)}(\xi, \zeta, \tau) + \dots \} \\ u^{(2)}(\xi, \zeta, \tau) &= \frac{1}{\epsilon} \{ u_0^{(2)}(\xi, \zeta, \tau) + \epsilon u_1^{(2)}(\xi, \zeta, \tau) + \dots \} \\ w^{(2)}(\xi, \zeta, \tau) &= w_0^{(2)}(\xi, \zeta, \tau) + \epsilon w_1^{(2)}(\xi, \zeta, \tau) + \dots \\ p^{(i)}(\xi, \zeta, \tau) &= \frac{1}{\epsilon} \{ p_0^{(i)}(\xi, \zeta, \tau) + \epsilon p_1^{(i)}(\xi, \zeta, \tau) + \dots \} \end{aligned}$$

These expansions follow the work done by Tilley et al [30] and Segin et al [27] but those works did not include slip on the boundary as well as gas compressibility and scaling of the viscosities and densities. However the formulation of the expansion allows for a cleaner investigation of the leading order terms so we will maintain this method. We then substitute these expansions into (1.18) - (1.23) and collect with regards to order. Here we separate the two problems into the respective cases mentioned above and solve to achieve our base state velocities, pressure and interface for each case.

### 3.1 Liquid-Liquid

Since we do not have compressibility effects to account for, this case is "simpler" than the general problem. The results are worth analysis and for this reason are included here. Once the above perturbations are substituted and collected by order we arrive at the following system of equations and boundary conditions:

$$O(\epsilon^{-1}) : p_{0\zeta}^{(i)} = 0 \quad (26)$$

$$\underline{\zeta = h(\xi, \tau)} : p_0^{(1)} = p_0^{(2)} \quad (27)$$

$$u_0^{(2)} = 0 \quad (28)$$

$$O(1) : -p_{0\xi}^{(2)} + \mu u_{0\xi\xi}^{(2)} = 0 \quad (29)$$

$$-p_{0\xi}^{(1)} + \sin \alpha + u_{0\zeta\zeta}^{(1)} = 0 \quad (30)$$

$$p_{1\zeta}^{(1)} + \cos \alpha = 0 \quad (31)$$

$$p_{1\zeta}^{(2)} = 0 \quad (32)$$

$$u_{0\xi}^{(1)} + w_{0\zeta}^{(1)} = 0 \quad (33)$$

$$u_1^{(2)} - u_0^{(1)} = 0 \quad (34)$$

$$u_{0\xi}^{(2)} + w_{0\zeta}^{(2)} = 0 \quad (35)$$

$$\underline{\zeta = h(\xi, \tau)} : u_0^{(2)} - u_0^{(1)} = 0 \quad (36)$$

$$\mu u_{0\zeta}^{(2)} - u_{0\zeta}^{(1)} = 0 \quad (37)$$

$$p_1^{(1)} - p_1^{(2)} = -Sh_{\xi\xi} \quad (38)$$

$$w_0^{(2)} - h_{\xi} u_0^{(2)} = 0 \quad (39)$$

$$\underline{\zeta = 0} : u_0^{(1)} = \beta_1 u_{0\zeta}^{(1)} \quad (40)$$

$$w_0^{(1)} = 0 \quad (41)$$

$$\underline{\zeta = 1} : u_0^{(2)} = -\beta_2 u_{0\zeta}^{(2)} \quad (42)$$

$$w_0^{(2)} = 0 \quad (43)$$

We find that that

$$p_0^{(1)}(\xi, \tau) = p_0^{(2)}(\xi, \tau) = p_0(\xi, \tau)$$

From O(1) we can also derive the pressure correction,  $p_1$  from the following:

$$\begin{aligned} p_1^{(1)}(\xi, \zeta, \tau) &= -(\cos \alpha)\zeta + p_1(\xi, \tau) \\ p_2^{(2)}(\xi, \tau) &= -h(\xi, \tau) \cos \alpha + p_1(\xi, \tau) + Sh_{\xi\xi} \end{aligned}$$

The momentum and continuity equations coupled with the appropriate boundary conditions give the following velocity equations for  $U_0^{(i)}$ :

$$u_0^{(1)} = \frac{\zeta^2}{2}(p_{0\xi} - \sin \alpha) + \left\{ \frac{-p_{0\xi} f_1}{2a_2} + h \sin \alpha \right\} (\zeta + \beta_1) \quad (44)$$

$$\begin{aligned} w_0^{(1)} &= -\frac{p_{0\xi\xi}}{6}\zeta^3 - \zeta \left( \frac{\zeta}{2} + \beta_1 \right) \\ &\quad \left\{ \frac{p_{0\xi\xi} f_1}{2f_2} - h_\xi \sin \alpha + \frac{p_{0\xi} h_\xi}{2} \left( \frac{2}{f_2} - \frac{f_1}{(f_2)^2} \right) \right\} \end{aligned} \quad (45)$$

$$u_0^{(2)} = \frac{p_{0\xi}}{2\mu} \left\{ \zeta^2 - 2\beta_2 - 1 - \frac{f_1(\zeta - \beta_2 - 1)}{f_2} \right\} \quad (46)$$

$$\begin{aligned} w_0^{(2)} &= \frac{-p_{0\xi\xi}\zeta^3}{6\mu} - \frac{p_{0\xi\xi} \left( -\frac{3}{2}h^2 + 3\beta_2 + \frac{3}{2} \right)}{6\mu f_2} + \\ &\quad \frac{p_{0\xi} h_\xi f_3}{4\mu} \left( \zeta^2 + \frac{(-2\beta_2 - 2)\zeta}{f_2} \right) \end{aligned} \quad (47)$$

where we have the following for  $f_1$ ,  $f_2$  and  $f_3$

$$\begin{aligned} f_1 &= (h^2 - 2\beta_2 - 1) \\ f_2 &= (h - \beta_2 - 1) \\ f_3 &= \frac{(h - 1)(h - 2\beta_2 - 1)}{h - \beta_2 - 1} \end{aligned}$$

Recall that  $S = \epsilon^2\sigma$  and indicates that the capillary forces are large when compared with the hydrostatic forces. We then use the following integral constraint:

$$\int_0^1 u_0 d\zeta = Q$$

where  $Q$  is the scaled constant flow rate. This gives the following equation for the pressure gradient  $p_{0\epsilon}$ :

$$\frac{12\mu f_2(-\frac{h^3}{3} \sin \alpha + Q)}{f_4\mu - h^4 - h^3(-4\beta_2 - 4) + h^2(-12\beta_2 - 6) + h(4 + 12\beta_2) - 4\beta_2 - 1} \quad (48)$$

such that  $f_4$  is

$$f_4 = h^4 + 6h^2(-\beta_2 - \frac{1}{2}) - 2h^3(-\beta_2 - 1)$$

Similarly, we arrive at the leading order interfacial equation by integrating  $u_0^{(i)}$  from 0 to 1 and achieve

$$h_\epsilon h^2 \sin \alpha + p_{0\epsilon} A_1 \quad (49)$$

where  $A_1$  is

$$\frac{hh_\epsilon \left( (\frac{1}{2} + \frac{1}{2}\beta_2)h^3 + (-\frac{1}{2} - 2\beta_2)h^2 + (-\frac{3}{2}\beta_2 - \frac{1}{2})h + \frac{1}{2} + 3\beta_2 + 4\beta_2^2 \right)}{(h - \beta_2 - 1)(h - 1)(h - 4\beta_2 - 1)}$$

We can continue this analysis up to order epsilon and get the following full equations for the interface:

$$h_t + h_\epsilon h^2 \sin \alpha + p_{0\epsilon} A_1 + \epsilon \left\{ \frac{h^3}{6} (Sh_{\xi\xi\xi} - 2h_\xi \cos(\alpha)) + C_1 \frac{h^2}{2} \right\}_\xi = 0 \quad (50)$$

and where  $C_1$  is as it is defined below.

$$C_1 = \frac{-p_{0\epsilon} f_1}{2f_2} + \frac{h^2 \mu (p_{0\epsilon} - \sin \alpha)}{f_2} + \frac{\mu (h + \beta_1)}{f_2} \left\{ \frac{p_{0\epsilon} f_1}{f_2} + h \sin \alpha \right\}$$

## 3.2 Liquid-Gas

We now turn to the more general case when the phase 2 fluid is a gas. Thus we must incorporate an equation of state and consider the effect compressible gas has on the derivation of the equations. This gives us the following system of equations up to the leading order with respective boundary conditions sections underlined:

$$O(\epsilon^{-1}) : p_{0\zeta}^{(i)} = 0 \quad (51)$$

$$\underline{\zeta = h(\xi, \tau)} : p_0^{(1)} = p_0^{(2)} \quad (52)$$

$$O(1) : -p_{0\xi}^{(2)} + \mu u_{0\xi\xi}^{(2)} = 0 \quad (53)$$

$$-p_{0\xi}^{(1)} + \sin \alpha + u_{0\zeta\zeta}^{(1)} = 0 \quad (54)$$

$$p_{1\zeta}^{(1)} + \cos \alpha = 0 \quad (55)$$

$$p_{1\zeta}^{(2)} = 0 \quad (56)$$

$$u_{0\xi}^{(1)} + w_{0\zeta}^{(1)} = 0 \quad (57)$$

$$u_1^{(2)} - u_0^{(1)} = 0 \quad (58)$$

$$\left(\rho u_0^{(2)}\right)_\xi + \left(\rho w_0^{(2)}\right)_\zeta = 0 \quad (59)$$

$$\underline{\zeta = h(\xi, \tau)} : u_0^{(2)} = 0 \quad (60)$$

$$\mu u_{0\zeta}^{(2)} - u_{0\zeta}^{(1)} = 0 \quad (61)$$

$$p_1^{(1)} - p_1^{(2)} = -Sh_{\xi\xi} \quad (62)$$

$$w_0^{(2)} - h_\xi u_0^{(2)} = 0 \quad (63)$$

$$\underline{\zeta = 0} : u_0^{(1)} = \beta_1 u_{0\zeta}^{(1)} \quad (64)$$

$$w_0^{(1)} = 0 \quad (65)$$

$$\underline{\zeta = 1} : u_0^{(2)} = -\beta_2 u_{0\zeta}^{(2)} \quad (66)$$

$$w_0^{(2)} = 0 \quad (67)$$

Thus using the above equations and boundary conditions we arrive at the following values for  $u_0^{(i)}$ :

$$u_0^{(1)} = \frac{\zeta^2}{2}(p_{0\xi} - \sin \alpha) + \left\{ \frac{-p_{0\xi} f_1}{2f_2} + h \sin \alpha \right\} (\zeta + \beta_1) \quad (68)$$

$$u_0^{(2)} = \frac{p_{0\xi}}{2\mu} \left\{ \zeta^2 - 2\beta_2 - 1 - \frac{f_1(\zeta - \beta_2 - 1)}{f_2} \right\} \quad (69)$$

We should note that these equations are identical to the liquid-liquid problem as they should be since the phase 1 fluid is identical in both models. However, when we use continuity and derive the equations for our phase 2 base state velocities  $w_0^{(i)}$  we see that the result of incorporating *rho*

$$w_0^{(1)} = -\frac{p_{0\xi\xi}}{6}\zeta^3 - \zeta \left( \frac{\zeta}{2} + \beta_1 \right) \left\{ \frac{p_{0\xi\xi} f_1}{2f_2} - h_\xi \sin \alpha + \frac{p_{0\xi} h_\xi}{2} \left( \frac{2}{f_2} - \frac{f_1}{(f_2)^2} \right) \right\} \quad (70)$$

$$w_0^{(2)} = -\left\{ \frac{p_{0\xi\xi}\rho}{2\mu} + \frac{\rho_\xi p_{0\xi}}{2\mu} \right\} \left\{ \frac{\zeta^3}{3} - 2\beta_2\zeta - \zeta - f_3 \right\} - \frac{\rho p_{0\xi} h_\xi}{2\mu} \left\{ \frac{2h h_\xi \left( \frac{\zeta^2}{2} - \beta_2 - \zeta \right)}{f_2} + f_5 \right\} \quad (71)$$

With the following for  $f_4$

$$f_4 = \frac{(h^2 - 2\beta_2 - 1) \left( \frac{\zeta^2}{2} - \beta_2\zeta - \zeta \right)}{h - \beta_2 - 1}$$

We then continue the analysis up to  $O(\epsilon)$  where we have:

$$\text{Re}_1[u_{0\tau}^{(1)} + u_0^{(1)}u_{0\xi}^{(1)} + u_{0\zeta}^{(1)}w_0^{(1)}] = -p_{1\xi}^{(1)} + u_{1\zeta\zeta}^{(1)} \quad (72)$$

$$\text{Re}_1\rho[u_0^{(2)}u_{0\xi}^{(2)} + u_{0\zeta}^{(2)}w_0^{(2)}] = -p_{1\xi}^{(2)} + \mu u_{1\zeta\zeta}^{(1)} \quad (73)$$

$$u_{1\xi}^{(1)} + w_{1\zeta}^{(1)} = 0 \quad (74)$$

$$\rho_t + \left(\rho u_1^{(2)}\right)_\xi + \left(\rho w_1^{(2)}\right)_\zeta = 0 \quad (75)$$

$$\underline{\zeta = 0} : u_1^{(1)} = \beta_1 u_{1\zeta}^{(1)} \quad (76)$$

$$w_1^{(1)} = 0 \quad (77)$$

$$\underline{\zeta = 1} : u_1^{(2)} = -\beta_2 u_{1\zeta}^{(2)} \quad (78)$$

$$w_1^{(2)} = 0 \quad (79)$$

$$\underline{\zeta = h} : \mu u_{1\xi}^{(2)} - u_{1\xi}^{(1)} = 0 \quad (80)$$

$$w_1^{(2)} - h_\xi u_1^{(2)} - w_0^{(1)} - h_\xi u_0^{(1)} = 0 \quad (81)$$

So by using (105) - (114) we arrive at the following solution for  $u_1^{(i)}$

$$u_1^{(1)} = \frac{\zeta^2}{2} p_{1\xi}^{(1)} + F^{(1)} + (\zeta + \beta_1) \left\{ \mu F_\zeta^{(2)}(\xi, h, \tau) - F_\zeta^{(1)}(\xi, h, \tau) + C_2 \right\} \quad (82)$$

$$u_1^{(2)} = \frac{\mu p_{1\xi}^{(2)}}{2} (\zeta^2 - 2\beta_2 - 1) + \mu F^{(2)} + (\zeta - \beta_2 - 1)C_2 \quad (83)$$

with  $C_2$  below:

$$C_2 = \frac{-p_{1\xi}^{(2)} f_1}{2f_2} + \frac{\mu h(h + 2\beta_1 \sin(\alpha) + h^2 \mu p_{0\xi})}{2f_2} - \frac{\mu f_1(h + \beta_1) p_{0\xi}}{2f_2^2} - \frac{\mu F_\zeta^{(2)}(\xi, h, \tau)}{f_2}$$

We now turn to derive the equations due to inertial effects, written above as  $F^{(1)}$  and  $F^{(2)}$ . We can do this from the first order velocity equations. For phase one we begin with

$$F_{\zeta\zeta}^{(1)}(\xi, \zeta, \tau) = \text{Re}_l \left[ u_{0\tau}^{(1)} + u_0^{(1)}u_{0\xi}^{(1)} + w_0^{(1)}u_{0\zeta}^{(1)} \right] \quad (84)$$

with the following boundary equations

$$F^{(1)}(\xi, 0, \tau) = 0 \quad (85)$$

$$F_{\zeta}^{(1)}(\xi, 0, \tau) = 0 \quad (86)$$

Note if we did not assume  $\beta_1$  is identically 0 we would have an additional term. After integrating the above and using our boundary conditions we arrive at the following:

$$F^{(1)}(\xi, \zeta, \tau) = a_1^{(1)}\zeta^6 + a_2^{(1)}\zeta^5 + a_3^{(1)}\zeta^4 + a_4^{(1)}\zeta^3 \quad (87)$$

where

$$a_1^{(1)} = \text{Re}_l \frac{p_{0\xi\xi}}{360} (p_{0\xi} - \sin \alpha)$$

$$a_2^{(1)} = \text{Re}_l \frac{p_{0\xi\xi}}{60} \left( h \sin \alpha - \frac{p_{0\xi} f_1}{2f_2} \right)$$

$$a_3^{(1)} = \frac{\text{Re}_l}{24} \left\{ p_{0\xi\tau} + \left[ h \sin \alpha - \frac{p_{0\xi} f_1}{2f_2} \right] \left[ \frac{p_{0\xi\xi} f_1}{2f_2} - h_{\xi} \sin \alpha + \frac{p_{0\xi} h_{\xi}}{2} \left( \frac{2}{f_2} - \frac{f_1}{f_2} \right) \right] \right\}$$

$$a_4^{(1)} = \frac{\text{Re}_l}{12} \left\{ 2h_{\tau} \sin \alpha - \frac{p_{0\xi\xi} f_1}{2f_2} + \frac{p_{0\xi} h_{\xi}}{2} \left( \frac{2}{f_2} - \frac{f_1}{f_2} \right) \right\}$$

For phase 2 we have a similar derivation, We now turn to derive the equations due to inertial effects, written above as  $F^{(1)}$  and  $F^{(2)}$ . We can do this from the first order velocity equations. For phase one we begin with

$$F_{\zeta\zeta}^{(2)}(\xi, \zeta, \tau) = \text{Re}_l \frac{\rho}{\mu} \left[ u_0^{(2)} u_{0\xi}^{(2)} + w_0^{(2)} u_{0\zeta}^{(2)} \right] \quad (88)$$

with the following boundary equations

$$F^{(2)}(\xi, 1, \tau) = 0 \quad (89)$$

$$F_{\zeta}^{(2)}(\xi, 1, \tau) = 0 \quad (90)$$

After integrating the above and using our boundary conditions we arrive at the following:

$$F^{(2)}(\xi, \zeta, \tau) = a_1^{(2)}(\zeta - 1)^6 + a_2^{(2)}(\zeta - 1)^5 + a_3^{(2)}(\zeta - 1)^4 - a_4^{(2)}\beta_2 \quad (91)$$

with

$$\begin{aligned}
a_1^{(2)} &= \text{Re}_l \frac{\rho p_{0\xi}}{120\mu^3} \left( \frac{h_\xi p_{0\xi} f_2}{f_1} - \frac{\rho_\xi}{\rho} p_{0\xi} \right) \\
a_2^{(2)} &= \text{Re}_l \frac{\rho p_{0\xi}}{80\mu^3} \frac{f_1}{f_2} \left( \frac{h_\xi p_{0\xi} f_2}{f_1} - \frac{\rho_\xi}{\rho} p_{0\xi} \right) \\
a_3^{(2)} &= \text{Re}_l \frac{\rho p_{0\xi}}{48\mu^3} \left( \frac{f_1}{f_2} \right)^2 \left( \frac{h_\xi p_{0\xi} f_2}{f_1} - \frac{\rho_\xi}{\rho} p_{0\xi} \right) \\
a_4^{(2)} &= \text{Re}_l \frac{\rho p_{0\xi}}{48\mu^3} \left( 2 - \frac{f_1}{f_2} \right) \left( \frac{h_\xi p_{0\xi} f_2 a_5^{(2)}}{f_1} - \frac{\rho_\xi}{\rho} p_{0\xi} a_6^{(2)} \right) \\
a_5^{(2)} &= \frac{(\zeta - 1)^4}{48} + \frac{f_1(\zeta - 1)^3}{f_2 24} + \frac{(\zeta - 1)^2}{4} + \frac{\zeta^4}{12} - \frac{\zeta^2}{2} + \frac{2\zeta}{3} + \frac{1}{12} \\
a_6^{(2)} &= \frac{(\zeta - 1)^4}{48} + \frac{f_1(\zeta - 1)^3}{f_2 24} + \frac{(\zeta - 1)^2}{8} \\
&\quad + \left( \frac{f_1}{f_2} \right)_\xi \frac{1}{h_\xi} \left[ \frac{(\zeta^2 - 1)^2}{16(2 - \frac{f_1}{f_2})} - \frac{f_1(\zeta - 1)^2(2 - f_1)}{8} + \frac{f_1(\zeta - 1)^2}{2 - f_1} \right]
\end{aligned}$$

We then integrate  $u^{(i)}$  with respect to  $\zeta$  from 0 to 1 to arrive at the pressure equation and use (1.17) to gain the interfacial equation. The interfacial equation is

$$\begin{aligned}
h_t + h_\xi h^2 \sin \alpha + \frac{p_{0\xi} \rho_\xi f_7}{12\rho f_2} - \frac{h_\xi p_{0\xi} f_5}{(h - 1)f_2 f_6} + \\
\epsilon \left\{ \frac{h^3}{6} (Sh_{\xi\xi\xi} - 2h_\xi \cos(\alpha)) + A_2 + \text{Re}_l I \right\}_\xi = 0 \quad (92)
\end{aligned}$$

while the pressure equation becomes

$$\begin{aligned}
\left( \frac{-p_{0\xi} \rho (1 - h)^3 (f_6)}{12(f_2)} \right)_\xi + \epsilon \left\{ \left( \frac{-p_{1\xi}^{(2)} \rho (1 - h)^3 (f_6)}{12(f_2)} \right)_\xi \right\} + \\
\epsilon \left\{ \rho_\tau (1 - h) + \frac{\sin \alpha h (1 - h) (f_1)}{4(f_2)} \left( \rho_\xi h + \frac{h_\xi \rho (f_1)}{f_2} \right) + \text{Re}_l T \right\} = 0 \quad (93)
\end{aligned}$$

where

$$\begin{aligned}
A_2 &= \frac{h^2}{4} \left\{ \frac{\mu h^2 (\sin(\alpha) + p_{0\xi})}{f_2} - \frac{\mu p_{0\xi} h f_1}{f_2^2} \right\} \\
I &= a_1^{(1)} \left( -\frac{20h^7}{7} \right) + a_2^{(1)} \left( -\frac{7h^6}{3} \right) + a_3^{(1)} \left( -\frac{9h^5}{5} \right) + a_2^{(1)} \left( -\frac{5h^4}{4} \right) \\
&+ a_1^{(2)} \frac{h^2}{2} \mu \left( 6(h-1)^5 - \frac{f_1}{f_2} (h-1)^6 \right) + a_2^{(2)} \frac{h^2}{2} \mu \left( 5(h-1)^4 - \frac{f_1}{f_2} (h-1)^5 \right) \\
&+ a_3^{(2)} \frac{h^2}{2} \mu \left( 4(h-1)^3 - \frac{f_1}{f_2} (h-1)^4 \right) - \beta_2 \frac{h^2}{2} \mu \left( \frac{\text{Re} \ell \rho p_{0\xi}}{\mu^3} \right) \left( 2 - \frac{f_1}{f_2} \right) \times \\
&\left\{ \frac{h_\xi p_{0\xi} f_2}{f_1} \left( a_{5\zeta}^{(2)} - \frac{f_1}{f_2} a_5^{(2)} \right) \Big|_{\zeta=h} + \frac{\rho_\xi}{\rho} p_{0\xi} \left( a_{6\zeta}^{(2)} - \frac{f_1}{f_2} a_6^{(2)} \right) \Big|_{\zeta=h} \right\} \\
T &= \frac{\mu a_1^{(2)} (-h-1)^7}{7} + \frac{\mu a_2^{(2)} (-h-1)^6}{6} + \frac{\mu a_3^{(2)} (-h-1)^5}{5} \\
&- \mu \beta_2 \left( \frac{\text{Re} \ell \rho p_{0\xi}}{\mu^3} \right) \left( 2 - \frac{f_1}{f_2} \right) \left\{ \frac{h_\xi p_{0\xi} f_2 A_3}{f_1} + \frac{\rho_\xi}{\rho} p_{0\xi} A_4 \right\} \\
&+ a_1^{(1)} \left( -\frac{20h^7}{7} \right) + a_2^{(1)} \left( -\frac{7h^6}{3} \right) + a_3^{(1)} \left( -\frac{9h^5}{5} \right) + a_2^{(1)} \left( -\frac{5h^4}{4} \right) \\
&+ \mu a_1^{(2)} A_5 \left( 6(h-1)^5 - \frac{f_1}{f_2} (h-1)^6 \right) + \mu a_2^{(2)} A_5 \left( 5(h-1)^4 - \frac{f_1}{f_2} (h-1)^5 \right) \\
&+ \mu a_3^{(2)} A_5 \left( 4(h-1)^3 - \frac{f_1}{f_2} (h-1)^4 \right) - \beta_2 \frac{h^2}{2} \mu \left( \frac{\text{Re} \ell \rho p_{0\xi}}{\mu^3} \right) \left( 2 - \frac{f_1}{f_2} \right) \times \\
&\left\{ \frac{h_\xi p_{0\xi} f_2}{f_1} \left( a_{5\zeta}^{(2)} - \frac{f_1}{f_2} a_5^{(2)} \right) \Big|_{\zeta=h} + \frac{\rho_\xi}{\rho} p_{0\xi} \left( a_{6\zeta}^{(2)} - \frac{f_1}{f_2} a_6^{(2)} \right) \Big|_{\zeta=h} \right\} \\
A_3 &= \frac{(-h-1)^5}{240} + \frac{(-h-1)^4}{f_2 96} + \frac{(-h-1)^3}{12} - \frac{h^5}{60} + \frac{h^3}{6} - \frac{h^2}{3} - \frac{h}{12} \\
A_4 &= \frac{((-h-1)^5}{240} + \frac{(-h-1)^4}{f_2 96} + \frac{(-h-1)^3}{24} \\
&+ \frac{f_1}{f_2 \xi h_\xi} \left\{ \frac{-h^4}{6} + \frac{h^2 - \frac{5}{6}}{32(2 - \frac{f_1}{f_2})} - \frac{f_1(-h-1)^3(2-f_1)}{24} + \frac{f_1(-h-1)^3}{3(2-f_1)} \right\}
\end{aligned}$$

$$A_5 = \frac{h^2}{2} + \frac{(-h-1)^2}{2f_2} - \beta_2 h$$

$$f_5 = h\{(-\beta_2 - 1)h^3 + (1 + 4\beta_2)h^2 + (1 + 3\beta_2)h - 1 - 8\beta_2^2 - 6\beta_2\}$$

$$f_6 = h - 4\beta_2 - 1$$

$$f_7 = h^2\{h^2 + (2 + 2\beta_2)h - 6\beta_2 - 3\}$$

We once again assume the volumetric flow rate is constant and use

$$\int_0^1 u \, dz = Q$$

which allows us to solve for  $P_{0\xi}$  in terms of  $h$  and  $Q$ . Thus we get

$$p_{0\xi} = \frac{Q + G \sin \alpha P_1}{P_2} \quad (94)$$

where

$$\begin{aligned} P_1 &= \frac{h^3}{6} + \frac{h^3 - 1}{6\mu} + \frac{(h-1)(2\beta_2 - 1)}{2\mu} + \left( \frac{(h-1)(h-2\beta_2 - 1)}{4\mu} + \frac{h^2}{4} \right) \times \\ &\quad \left( \frac{\mu h^2 - (h^2 - 2\beta_2 - 1)}{h(1-\mu) - \beta_2 - 1} \right) \\ P_2 &= \left( \frac{(h-1)(h-2\beta_2 - 1)}{4\mu} + \frac{h^2}{4} \right) \times \\ &\quad \left( \frac{\rho(h^2 - 2\beta_2 - 1) - \mu h^2 - 2h(h - \beta_2 - 1)(\rho - 1)}{h(1-\mu) - \beta_2 - 1} \right) - \frac{h^3}{6} \\ &\quad + \frac{h(\rho - 1)(h-1)(h-2\beta_2 - 1)}{2\mu} - \rho \left( \frac{h^3 - 1}{6\mu} + \frac{(h-1)(2\beta_2 - 1)}{2\mu} \right) \end{aligned}$$

## 4 Long Wave Linear Stability Analysis

### 4.1 Analysis of the Liquid-Liquid Case

For the liquid-liquid case we recall that we assumed the volumetric flow rate,  $Q$  to be included in the pressure gradient. This allowed us to substitute functions of  $h$  and  $Q$  in for our pressure throughout the derivation of the

interfacial equation. We then expand about the steady state solution of interface,  $h_0$ .

$$h(\xi, \tau) = h_0 + H_0 e^{ik(\xi - ct)}$$

We substitute these as well as our pressure gradient equation (1.3.23) into (1.3.25) and arrive at the following characteristic equation:

$$\begin{aligned} &(-cik)H_0 + g_1(ik)H_0 + g_2(ik)^2H_0 - g_3(ik)^4 + g_5(ik)H_0 - \\ &g_6(ik)H_0 + g_7(ik)H_0 + g_9(ik)H_0 - g_{10}(ik)H_0 \end{aligned} \quad (95)$$

Note that  $k$  is the wave number and the imaginary part of  $kc$  gives the growth rate and stability information. This gives us the following solutions:

$$kc_i = k^2 [g_2 - k^2 g_3] \quad (96)$$

$$kc_r = k [g_1 + g_5 - g_6 + g_7 + g_9 - g_{10}] \quad (97)$$

The coefficients are functions of  $h$  and  $Q$  and are as follows:

$$g_1 = h_0^2 \sin \alpha$$

$$g_2 = \frac{-\epsilon h_0^2 \cos \alpha (h_0^2 - 2\beta_2 - 1)}{4(h_0 - \beta_2 - 1)}$$

$$g_3 = \frac{\epsilon S h_0^2 (h_0^2 - 2\beta_2 - 1)}{4(h_0 - 2\beta_2 - 1)}$$

$$g_5 = \frac{3\mu h_0 \left( Q - \frac{h_0^3}{3} \sin \alpha \right) (h_0^3 + g'_5 h_0 + 4\beta_2^2 + 2 + 6\beta_2)}{f_1(\mu - 1)(h_0^4 - g''_5 + 6(\mu + 2)(-\beta_2 - \frac{1}{2})h_0^2 + (4 + 12\beta_2)h_0 - 4\beta_2 - 1)}$$

$$g'_5 = (6\beta_2 - 2\beta_2^2 - 3)$$

$$g''_5 = 2(-\beta_2 - 1)(\mu + 2)h_0^3$$

$$g_6 = \frac{6\mu^2 h_0^2 \left( Q - \frac{h_0^3}{3} \sin \alpha \right) g'_6}{f_1^2(\mu - 1)(h_0^4 - g''_5 + 6(\mu + 2)(-\beta_2 - \frac{1}{2})h_0^2 + (4 + 12\beta_2)h_0 - 4\beta_2 - 1)}$$

$$g'_6 = (-\beta_2 - 1)h_0^2 + \left( 2\beta_2^2 + \frac{5}{2} + 5\beta_2 \right) h_0 - \frac{3}{2} - \frac{9}{2}\beta_2 - 3\beta_2^2$$

$$g_7 = \frac{3\mu h_0^3 \left(h_0 - \frac{4}{3}\beta_2 - \frac{4}{3}\right) \sin \alpha}{4(h_0 - \beta_2 - 1)^2}$$

$$g_8 = \frac{3 \cos \alpha h_0 g'_8}{4(h_0 - \beta_2 - 1)^2}$$

$$g'_8 = h_0^3 + \left(-\frac{4}{3}\beta_2 - \frac{4}{3}\right) h_0^2 + \left(-\frac{2}{3}\beta_2 - \frac{1}{3}\right) h_0 + \frac{4}{3}\beta_2^2 + \frac{2}{3} + 2\beta_2$$

$$g_9 = \frac{h_0^2 + (2 + 2\beta_2)h_0 - 6\beta_2 - 3}{12(h_0 - \beta_2 - 1)} Q'$$

$$g_{10} = \frac{h_0^3 \mu ((-\beta_2 - 1)h_0 + 1 + 2\beta_2)}{4(h_0 - \beta_2 - 1)^2} Q'$$

$$Q' = \frac{\mu h_0 Q'' - 12 f_1 \mu h_0^2 \sin \alpha}{f_1(\mu - 1)(h_0^4 - g_5'' + 6(\mu + 2)(-\beta_2 - \frac{1}{2})h_0^2 + (4 + 12\beta_2)h_0 - 4\beta_2 - 1)} + \frac{12 f_1 \mu Q'' (f_1(\mu - 1)(h_0^3 - 3g_5''/h_0 + 12(\mu + 2)(-\beta_2 - \frac{1}{2})h_0 + (4 + 12\beta_2))}{(f_1(\mu - 1)(h_0^4 - g_5'' + 6(\mu + 2)(-\beta_2 - \frac{1}{2})h_0^2 + (4 + 12\beta_2)h_0 - 4\beta_2 - 1))^2}$$

$$Q'' = \left(Q - \frac{h_0^3}{3} \sin \alpha\right)$$

Note that the imaginary part of the characteristic equation gives us the following result.

$$kc_i = -\epsilon k^2 \left[ \frac{h_0^2 \cos \alpha (h_0^2 - 2\beta_2 - 1)}{4(h_0 - \beta_2 - 1)} + \frac{Sh_0^2 (h_0^2 - 2\beta_2 - 1)k^2}{4(h_0 - 2\beta_2 - 1)} \right] \quad (98)$$

This characteristic equation is always stable when  $\text{Re} = 0$  as shown above. The first term is due to hydrostatics while the latter is the capillarity effects. We assume that  $\beta_2 \ll 1$  and so  $1 - h_0 - 2\beta_2 > 0$ . Similarly, we know that  $0 < h_0 < 1$  which implies that  $1 - h_0^2 > 1 - h_0$ . So both the hydrostatics and capillarity terms will always be greater or less than unity.

## 4.2 Analysis of Liquid-Gas Case

In order to examine if slip on the compressible fluid wall boundary has an affect on the interfacial dynamics we use the classical differential equation analysis method of Linear Stability Theory. We assume a steady state solution for the interface and pressure equations. We will also use the ideal gas

law and define  $P^{(2)} = D\rho$  where  $D = R_s T$ , the specific gas constant and local temperature of the gas respectively. So we have  $h_0$  and  $\rho_0$ , both constants and steady state solutions to our equations. We shall expand as follows:

$$h(\xi, \tau) = h_0 + H_0 e^{ik(\xi - ct)}$$

$$\rho(\xi, \tau) = \rho_0 + H_0 e^{ik(\xi - ct)}$$

We then substitute these into (1.3.35) and (1.3.36). Since we are considering  $\delta$  small we can then let  $\delta \implies 0$ . This gives the following system of characteristic equations:

$$a_1(ik)^2 \rho_0 + \epsilon(-cik)\rho_0 + a_2(ik)\rho_0 + a_3(ik)H_0 = 0 \quad (99)$$

$$\begin{aligned} &(-cik)H_0 + b_1(ik)H_0 + b_2(ik)^2 H_0 + b_3(ik)^4 H_0 - b_4(ik)^2 + b_5(ik)^2 \\ &+ \rho_0 + b_6(ik)H_0 = 0 \end{aligned} \quad (100)$$

$k$  is the wave number and

$$a_1 = \frac{\rho_0(h_0 - 1)^3(h_0 - 4\beta_2 - 1)D}{6(h_0 - \beta_2 - 1)}$$

$$a_2 = \frac{\epsilon\rho_0 \sin \alpha(1 - h_0)(h_0 - 2\beta_2 - 1)}{4(h_0 - \beta_2 - 1)}$$

$$a_3 = \frac{\epsilon\rho_0 \sin \alpha h_0(1 - h_0)(h_0 - 2\beta_2 - 1)(h_0 - 2\beta_2 - 2)}{4(h_0 - 2\beta_2 - 1)^2}$$

$$b_1 = h_0^2 \sin \alpha$$

$$b_2 = \frac{-\epsilon h_0^2 \cos \alpha(h_0^2 - 2\beta_2 - 1)}{4(h_0 - \beta_2 - 1)}$$

$$b_3 = \frac{\epsilon S h_0^2(h_0^2 - 2\beta_2 - 1)}{4(h_0 - 2\beta_2 - 1)}$$

$$b_4 = \frac{\epsilon h_0^2(h_0^2 + (2 + 2\beta_2)h_0 - 6\beta_2 - 3)D}{12(h_0 - 2\beta_2 - 1)}$$

$$b_5 = \frac{\epsilon h_0^3 ((-\beta_2 - 1)h_0 + 1 + 2\beta_2)D}{4(h_0 - 2\beta_2 - 1)^2}$$

$$b_6 = \frac{\epsilon h_0^3 (3h_0 - 4\beta_2 - 4)}{4(h_0 - 2\beta_2 - 1)^2}$$

We then use the system of two coupled equations to find  $kc$ . The imaginary part of  $kc$  gives the growth rate and thus, a view of the stability after the system is given a small disturbance. We look at the case when  $D = 0$ . Here the interfacial perturbation does not depend on the density perturbation. However the density perturbation does depend on the interfacial perturbation. So in this special case, the interfacial dynamics determine the stability of the whole system. Thus our system of characteristic equations simplifies to:

$$\epsilon(-cik)\rho_0 + a_2(ik)\rho_0 + a_3(ik)H_0 = 0 \quad (101)$$

$$(-cik)H_0 + b_1(ik)H_0 + b_2(ik)^2H_0 + b_3(ik)^4H_0 + b_6(ik)H_0 = 0 \quad (102)$$

Reintroducing the inertial terms we find

$$kc_i = k^2 \left[ \frac{-\epsilon h_0^2 \cos \alpha (h_0^2 - 2\beta_2 - 1)}{4(h_0 - \beta_2 - 1)} - \frac{\epsilon S h_0^2 (h_0^2 - 2\beta_2 - 1) k^2}{4(h_0 - 2\beta_2 - 1)} + \epsilon \text{Re} \frac{2}{15} h_0^6 \sin^2 \alpha \right] \quad (103)$$

$$kc_r = k \left[ h_0^2 \sin \alpha - \frac{\epsilon h_0^3 (3h_0 - 4\beta_2 - 4)}{4(h_0 - 2\beta_2 - 1)^2} \right] \quad (104)$$

The analysis of the neutral stability curves in Figure 2 shows that for  $k < 0.5$  all  $0 < \beta < 1$  is stabilizing. This is further shown in Figure 3 by looking at the growth rate of  $kc_i$  as  $k$  gets larger with several values of  $\beta$ .

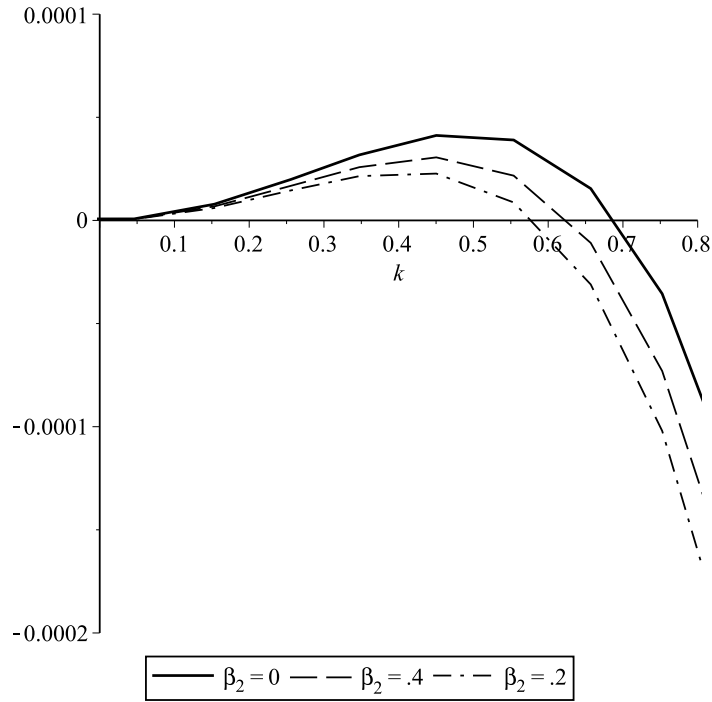


Figure 2: Stabilizing of  $k$  due to slip. The results above show the stabilizing effects of  $\beta$  where  $\text{Re} = 1$ ,  $\mu = 1$ ,  $S = 3$ ,  $h = 0.5$ ,  $\epsilon = 0.01$ ,  $\alpha = \frac{\pi}{4}$

The result is similar to the linear stability analysis of the fluid-fluid system when we consider the inertial terms identically equal to zero and suggests that the slip boundary condition should be stabilizing for small values of  $k$ . This creates the opposite result of the system without slip incorporated.

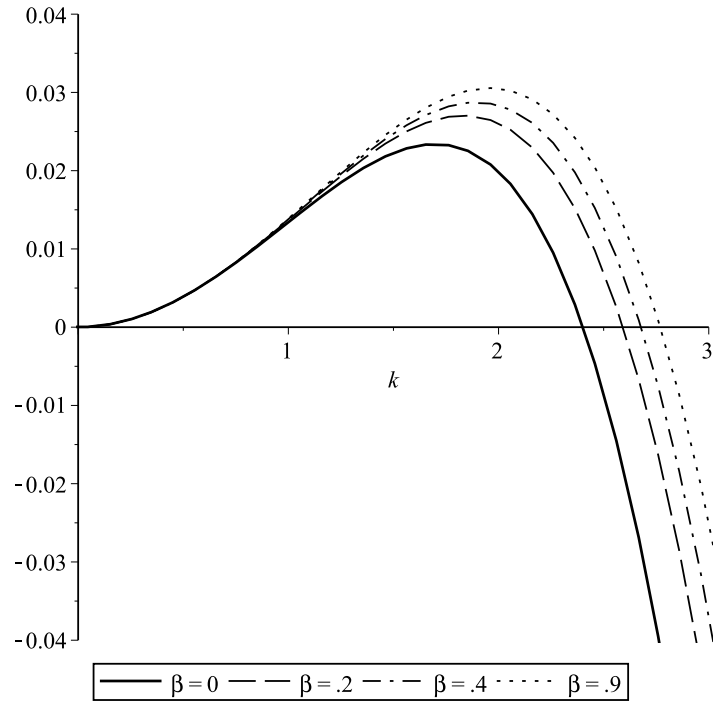


Figure 3: Stabilizing of  $k$  due to slip. The results above show the stabilizing effects of  $\beta$  where  $\text{Re} = 1$ ,  $\mu = 1$ ,  $S = 3$ ,  $h = 0.5$ ,  $\epsilon = 0.01$ ,  $\alpha = \frac{\pi}{4}$

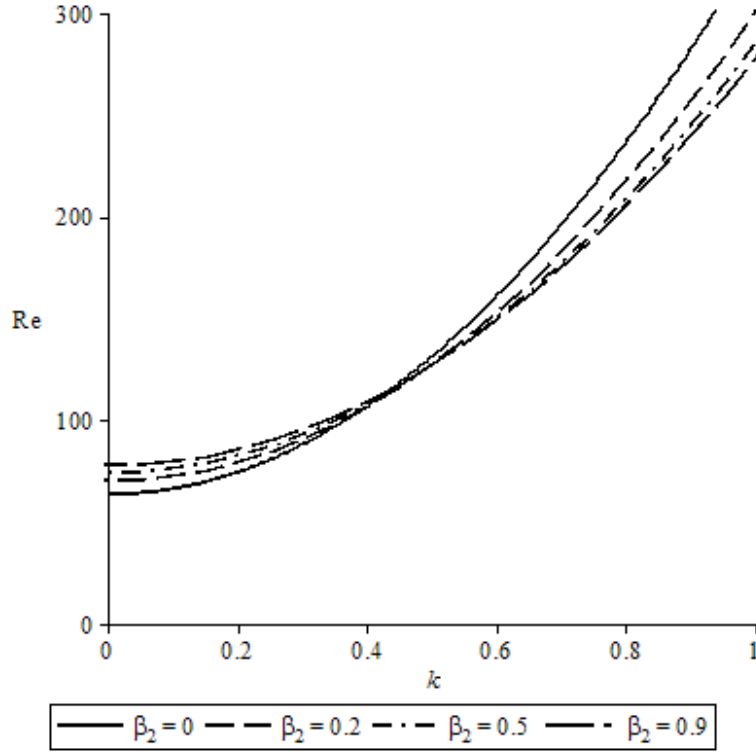


Figure 4: Neutral Stability curves of the effect of  $\beta$  on  $\text{Re}(k)$  when  $kc_i = 0$ ,  $\mu = 1$ ,  $S = 3$ ,  $h = 0.5$ ,  $\epsilon = 0.01$ ,  $\alpha = \frac{\pi}{4}$

## 5 Conclusion and Planned Future Work

In this paper, we introduced a Navier-slip boundary condition to the microchannel two fluid flow problem. We introduced dimensionless variables and by using perturbation theory we were able to analyze the problem based on different orders of investigation.

Looking at both the gas-fluid and fluid-fluid versions of the problem, we assumed a base state solution to the interface and pressure gradient. Using boundary conditions and equations of state, we were able to solve for the velocities of both the compressible and incompressible fluids. For the more complex system, we derived the interfacial conditions as well which fed the analytical results we eventually arrived at.

We showed that for small values of the slip coefficient  $\beta$ , slip is actu-

ally stabilizing to laminar flow which confirms an interesting phenomena explained in the introduction such as the work done by Vetcha et al [31]. This result was shown both for the neutral stability curves as well as the growth rate of  $k$ . This stabilization could be physically due to the reduction in friction outlined by Davis and Lauga [10].

Future work already outlined includes numerical analysis of the problem using a spectral method approach or finite difference algorithm. Utilizing the Orr-Sommerfeld derivation of the problem, we will further investigate the results found here and solidify the analytical prediction that slip is stabilizing for small values of  $\beta$  on one wall of the microchannel fluid system.

Furthermore, the problem is ideally setup to introduce slip on both the liquid-wall and the gas-wall surfaces so analysis of the entire system under slip conditions will be investigated as well. The impact of slip on the Rayleigh-Taylor instability shows investigation of this nature is required and could lead to original results. A weakly nonlinear analysis using the Kuramoto-Sivashinky form of the interfacial equation will also be performed.

## References

- [1] Instability of navier slip flow of liquids. *Comptes Rendus Mcanique*, 332(11):895 – 900, 2004.
- [2] Errol B. Arkhilic, Martin A. Schmidt, and Kenneth Breuer. Gaseous slip flow in long microchannels. *Journal of Microelectromechanical Systems*, 6(2):167–178, 1997.
- [3] R.W. Barber and D.R. Emerson. Analytical solution of low reynolds number slip flow past a sphere. *Science*, pages –00–001, 2000.
- [4] G.K. Batchelor. An introduction to fluid dynamics. 1967.
- [5] D.J. Benney. Long waves on liquid films. *Journal of Mathematical Physics*, 45(150):150–155, 1966.
- [6] A. Bertozzi, M. Shearer, and R. Buckingham. Thin film traveling waves and the navier slip condition. *SIAM Journal on Applied Mathematics*, 63(2):722–744, 2003.
- [7] A. B. D. Cassie and S. Baxter. Wettability of porous surfaces. *Trans. Faraday Soc.*, 40:546–551, 1944.
- [8] C. Cercignani. The boltzman equation and its applications. 1988.
- [9] Suman Chakraborty and Kumar Dinkar Anand. Implications of hydrophobic interactions and consequent apparent slip phenomenon on the entrance region transport of liquids through microchannels. *Physics of Fluids*, 20:043602, 2008.
- [10] Anthony M. Davis and Eric Lauga. Geometric transition in friction for flow over a bubble mattress. *Physics of Fluids*, 21:011701, 2009.
- [11] Zhipeng Duan and Y. Muzychka. Slip flow in non-circular microchannels. *Microfluidics and Nanofluidics*, 3:473–484, 2007. 10.1007/s10404-006-0141-4.
- [12] Zhipeng Duan and Y.S. Muzychka. Slip flow in elliptic microchannels. *International Journal of Thermal Sciences*, 46(11):1104 – 1111, 2007. [jce:titlejNano, Micro and Mini Channelsj/ce:titlej](#).

- [13] Zhipeng Duan and Y.S. Muzychka. Slip flow in the hydrodynamic entrance region of circular and noncircular microchannels. *Journal of Fluids Engineering*, 132:011201, 2010.
- [14] Dietrich Einzel, Peter Panzer, and Mario Liu. Boundary condition for fluid flow: Curved or rough surfaces. *Physical Review Letters*, 64(19):2269–2272, 1990.
- [15] François Feuillebois, Martin Z. Bazant, and Olga I. Vinogradova. Effective slip over superhydrophobic surfaces in thin channels. *Phys. Rev. Lett.*, 102:026001, Jan 2009.
- [16] Xiao-Jun Gu and D.R. Emerson. A high-order moment approach for capturing non-equilibrium phenomena in the transition regime. *Journal of Fluid Mechanics*, 636:177–216, 2009.
- [17] H.D. Madhawa Hettiarachchi, Mihajlo Golubovic, William M. Worek, and W.J. Minkowycz. Three-dimensional laminar slip-flow and heat transfer in a rectangular microchannel with constant wall temperature. *International Journal of Heat and Mass Transfer*, 51(2122):5088 – 5096, 2008.
- [18] Eric Lauga and Howard A. Stone. Effective slip in pressure-driven stokes flow. *Journal of Fluid Mechanics*, 489:55–77, July 2003.
- [19] Gian Luca Morini, Marco Lorenzini, and Marco Spiga. A criterion for experimental validation of slip-flow models for incompressible rarefied gases through microchannels. *Microfluidics and Nanofluidics*, 1:190–196, 2005. 10.1007/s10404-004-0028-1.
- [20] Y.S. Muzychka and M.M. Yovanovich. Pressure drop in laminar developing flow in noncircular ducts: A scaling and modeling approach. *Journal of Fluids Engineering*, 131:111105–1, 2009.
- [21] Chiu-On Ng and C. Wang. Apparent slip arising from stokes shear flow over a bidimensional patterned surface. *Microfluidics and Nanofluidics*, 8:361–371, 2010. 10.1007/s10404-009-0466-x.
- [22] Chiu-On Ng and C. Y. Wang. Stokes shear flow over a grating: Implications for superhydrophobic slip. *Physics of Fluids*, 21:013602, 2009.

- [23] M. Renksizbulut, H. Niazmand, and G. Tercan. Slip-flow and heat transfer in rectangular microchannels with constant wall temperature. *International Journal of Thermal Sciences*, 45(9):870 – 881, 2006.
- [24] M. Sbragaglia and A. Prosperetti. Effective velocity boundary condition at a mixed slip surface. *Journal of Fluid Mechanics*, 578:435–451, 2007.
- [25] Mauro Sbragaglia and Andrea Prosperetti. A note on the effective slip properties for microchannel flows with ultra-hydrophobic surfaces. *Physics of Fluids*, 19:043603, 2007.
- [26] T.M. Segin, L. Kondic, and B.S. Tilley. Long-wave linear stability theory for two-fluid channel flow including compressibility effects. *IMA Journal of Applied Mathematics*, 71:715–739, 2006.
- [27] T.M. Segin, B.S. Tilley, and L. Kondic. On undercompressive shocks and flooding in countercurrent two-layer flows. *Journal of Fluid Mechanics*, 532:217–242, 2005.
- [28] C. Teo and B. Khoo. Flow past superhydrophobic surfaces containing longitudinal grooves: effects of interface curvature. *Microfluidics and Nanofluidics*, 9:499–511, 2010. 10.1007/s10404-010-0566-7.
- [29] Kevin W. Tibbs, Florence Baras, and Alejandro L Garcia. Anomalous flow profile due to the curvature effect on slip length. *Physical Review*, 56(2):2282–2283, August 1997.
- [30] B.S. Tilley, S.H. Davis, and S.G. Bankoff. Linear stability theory of two-layer fluid flow in an inclined channel. *Physics of Fluids*, 6:3609–3922, 1994.
- [31] N. Vetcha, S. Smolentsev, and M. Abdou. Linear stability analysis for the hartmann flow with interfacial slip. *Magnetohydrodynamics*, 48(1):147 – 155, 2012.
- [32] Christophe Ybert, Catherine Barentin, Cécile Cottin-Bizonne, Pierre Joseph, and Lydric Bocquet. Achieving large slip with superhydrophobic surfaces: Scaling laws for generic geometries. *Physics of Fluids*, 19:123607, 2007.

- [33] Sun Yuhong, Robert W. Barber, and David R. Emerson. Inverted velocity profiles in rarefied cylindrical couette gas flow and the impact of the accomodation coefficient. *Physics of Fluids*, 17(047102):047102–1 – 047102–7, 2005.
- [34] Azad Qazi Zade, Metin Renksizbulut, and Jacob Friedman. Heat transfer characteristics of developing gaseous slip-flow in rectangular microchannels with variable physical properties. *International Journal of Heat and Fluid Flow*, 32(1):117 – 127, 2011.